Review

Special Issue – Imaging Cell Biology

Photoactivatable fluorescent proteins for diffraction-limited and super-resolution imaging

Jennifer Lippincott-Schwartz and George H. Patterson

Cell Biology and Metabolism Program, NICHD, NIH Bethesda, MD, USA

Photoactivatable fluorescent proteins (PA-FPs) are molecules that switch to a new fluorescent state in response to activation to generate a high level of contrast. Over the past eight years, several types of PA-FPs have been developed. The PA-FPs fluoresce green or red, or convert from green to red in response to activating light. Others reversibly switch between 'off' and 'on' in response to light. The optical ''highlighting'' capability of PA-FPs has led to the rise of novel imaging techniques providing important new biological insights. These range from *in cellulo* pulse-chase labeling for tracking subpopulations of cells, organelles or proteins under physiological settings, to super-resolution imaging of single molecules for determining intracellular protein distributions at nanometer precision. This review surveys the expanding array of PA-FPs, including their advantages and disadvantages, and highlights their use in novel imaging methodologies.

Introduction

By allowing the visualization of cells and their constituents, genetically-encoded fusions of fluorescent proteins (FPs) have provided an important tool for dissecting the molecular control of cellular processes within cells, spurring a revolution in biology [1]. The advent of PA-FPs [2–4] offers new capabilities, such as pulse-chase labeling and single molecule localizations. These capabilities are achieved because PA-FPs undergo pronounced changes in their spectral properties in response to irradiation with light of a specific wavelength and intensity. That is, activated molecules switched on by photoactivation yield bright signals over dark backgrounds. This enables the spatial and temporal marking of specific structures and tracking of their signal in time over a "dark" background. Because PA-FPs are 'switched on', measurements are not impacted by freshly synthesized molecules that become fluorescent, as occurs in imaging with conventional FPs.

The optical highlighting capability of PA-FPs, together with their ability to be expressed as fusion proteins that retain complex biological functions, has led to the development of diverse and novel imaging strategies. For example, pulse-chase labeling of cellular compartments using PA-FPs has helped clarify protein transport pathways and the intricate connections between compartments. Furthermore, by summing the locations of single molecules determined by the optical on/off switching of sparse subsets of PA-FPs and determining the centroids of their fluorescence emission, a final super-resolution image can be obtained, revealing the complex distributions of molecules within subcellular structures with nanometer precision. The full potential of PA-FPs in conventional, diffraction-limited and super-resolution imaging is only beginning to be realized. Here, we discuss the diverse array of PA-FPs available to researchers and the new imaging techniques they make possible for unraveling long-standing biological questions.

Palette of PA-FPs

Over 20 different varieties of PA-FPs have so far been described. As discussed below, these fall into three broad classes based on whether, in response to an activating light pulse, the PA-FP i) irreversibly switches from a dark-to-bright fluorescent state, ii) irreversibly photoconverts from one fluorescent color to another or iii) reversibly photoconverts, enabling on/off switching capability. Within these classes, individual PA-FPs can be further differentiated based on particular optical and biochemical characteristics (Table 1). These include their brightness level, oligomeric state, contrast ratio, rate of spontaneous conversion into an activated state and rate of photobleaching. The specific combination of these characteristics exhibited by a particular PA-FP makes it more or less suitable for various types of applications in diffraction-limited and super-resolution imaging.

The brightness of a PA-FP after it has been photoactivated is the product of the activated chromophore's extinc-

Glossary

Diffraction barrier: Limits resolution when imaging with a conventional fluorescence microscope to approximately 0.61 of the wavelength of light divided by the numerical aperture of the objective lens.

Point spread function (PSF): This defines the blurry, diffraction-limited spot given off by a single point source light emitter (i.e. PA-FP) when imaged through an objective lens. When the shape of the PSF is measured, its centroid can be determined with high precision providing 'super-resolution localization' of the point source light emitter. The precision with which the point source is localized scales approximately to the half-width of the PSF divided by the square root of the number of photons collected.

Corresponding author: Lippincott-Schwartz, J. (jlippin@helix.nih.gov)

0962-8924/$ – see front matter doi:10.1016/j.tcb.2009.09.003

Table 1. Example PA-FP on-state properties

PA-FP classes	ex (nm)	em (nm)	Brightness[a]	Oligomeric state	Contrast	Reference
Irreversible, off to on						
PAGFP	504	517	13750	monomer	70	[5]
PAmCherry1	564	595	8280	monomer	4000	[7]
Photoconversion, wavelength shift						
PS-CFP2	490	511	10810	monomer	>2000[b]	[21]
Kaede	572	582	19900	tetramer	2000[c]	[11]
KikGR	583	593	21200	tetramer	>2000[c]	[12]
mKikGR	580	591	17650	tetramer	NR	
Dendra2	553	573	19250	monomer	300	[14]
EosFP	571	581	22600	tetramer	NR	[13]
mEos2	573	584	30300	monomer	NR	[19]
Reversible photoactivation						
Dronpa	503	518	80800	monomer	NR	[30]
rsFastlime	496	518	30100	monomer	70[d]	[23]
Padron	396	522	27500	monomer	140[d]	[24]
KFP1	580	600	4100	tetramer	>30	[26]
rsCherry	572	610	1600	monomer	7[d]	[25]
rsCherryRev	572	608	420	monomer	20[d]	[25]

NR, not reported.
[a]Product of extinction coefficient and quantum yield.
[b]Determined by the green-to-cyan fluorescence ratio after photoactivation divided by the green-to-cyan fluorescence ratio before photoactivation.
[c]Determined by the red-to-green fluorescence ratio after photoactivation divided by the red-to-green fluorescence ratio before photoactivation.
[d]Determined by ratio of the maximum signal divided by the residual off-state fluorescence.

tion coefficient and quantum yield (i.e. ratio of photons emitted to photons absorbed). In general, the brightest PA-FP is most useful for all applications because brighter molecules emit more photons and thereby are easier to image. The contrast ratio (i.e. dynamic range) of a PA-FP is the ratio of its fluorescence before and after photoactivation. Variability in contrast ratios among PA-FPs is largely due to differences in their spontaneous photoconversion in the absence of controlled activation, which increases the background fluorescence during imaging. For this reason, a PA-FP with high contrast ratio is best for most imaging purposes. Photoactivated PA-FPs undergo photobleaching during imaging, which limits how long their signals can be observed. In most diffraction-limited imaging applications the less photobleaching the better. By contrast, in single molecule super-resolution imaging, because localized molecules must be bleached before others can be photoactivated (otherwise the signals from PA-FPs will overlap and not be separated by more than the diffraction limit of light), a balance between rate of photobleaching and photoactivation is desirable.

Dark-to-bright PA-FPs

These PA-FPs all initiate fluorescence emissions from a quiescent or dark state. PA-FPs in this class include PA-GFP, a photoactivatable variant of the *Aequorea victoria* green fluorescent protein (GFP), and PA variants derived from DsRed, including PAmRFP1 and PAmCherry1. PA-GFP, one of the first PA-FPs developed, is derived from wtGFP by the substitution of histidine to threonine at position 203 (T203H) [5]. Little green fluorescence is exhibited by PA-GFP until it is activated with intense violet light (390–415 nm). After irradiation, a 70-fold increase in green fluorescence (emission peak at 504 nm) is produced. The absence of fluorescence in its non-activated form gives PA-GFP a high dynamic range for imaging, but has a drawback in that selecting regions to photoactivate can be difficult with the small pre-photoactivation signal. Nevertheless, PA-GFP's overall brightness, photostability and fusion protein compatibility (i.e. it is monomeric) has made it popular.

PA-mRFP1 [6] and PAmCherry1 [7], both derived from DsRed, switch from dark to red upon illumination with intense violet light. They are monomeric and, thus, can be used as fusion tags. Because they emit red light, they are less phototoxic and easier to image in thick specimens than PA-FPs emitting green light. This makes them highly desirable in applications involving deep tissue or whole organism imaging. PAmCherry1 has a faster maturation rate, higher contrast ratio and greater quantum yield than PA-mRFP1, making it the preferable monomeric red PA-FP for use in both diffraction-limited and super-resolution imaging [7].

PAmCherry1 has been used together with PA-GFP in two-color photoactivation imaging [7]. The PAmCherry1/PA-GFP combination has proved effective because the respective red and green wavelengths of PAmCherry1 and PA-GFP do not overlap. That is, there is no green fluorescence from PAmCherry1 or red fluorescence from PA-GFP before or after photoactivation. Thus, in coexpressing cells, PAmCherry1 and PA-GFP can be switched on simultaneously from a dark state after a brief pulse of 405 nm laser and thereafter imaged using 564 nm and 488 nm irradiation. This characteristic makes the

PAmCherry1/PA-GFP combination particularly suitable for performing two-color photoactivation experiments in living cells. By contrast, other dual-color imaging approaches using PA-FPs with better contrast ratios require strategies involving switching between two states [8–10] and are not as straightforward for live cell conditions.

Irreversible photoconverters

PA-FPs in this class photoconvert from one fluorescence emission bandwidth to another. This enables tracking before photoconversion, so it is easy to select specific regions to photoactivate. The green-to-red highlighters in this class include EosFP, Kaede, KikGR and Dendra2, and are all derived from stony corals [11–14]. They contain a chromophore that initially emits green fluorescence. Irradiation with UV light causes irreversible peptide cleavage near the chromophore and the subsequent extension of the electron conjugation system, resulting in a new emission peak in the red spectrum [15,16].

One of the best overall performers among the green-to-red highlighters is EosFP [13]. It has high brightness, good contrast ratio and has been engineered into a monomeric form suitable for live cell imaging (i.e. mEosFP, dEosFP and tdEosFP). Of these, dEosFP and tdEosFP are preferable to mEosFP because the latter's chromophore formation requires temperatures below 30 °C, which limits its use to non-mammalian cells. EosFP has the highest photon output of all known photoconvertible FPs [8,17], explaining its frequent use in single molecule super-resolution imaging. The simultaneous decrease of green and increase in red fluorescence emission upon photoactivation of EosFP further can be exploited in a ratiometric analysis using two-channel detection, yielding a factor of 2000 in the ratio of green-to-red fluorescence. Two-color, diffraction-limited imaging with EosFP is also possible by coexpressing it with a fusion protein containing EGFP [18]. After Eos-FP is photoconverted to red, each protein is visibly distinct and can be imaged over time. A drawback to this approach is that any tdEosFP not converted at the start of the experiment or that is synthesized during the course of the experiment will fluoresce green, potentially complicating interpretations. A recent improvement in mEosFP, termed mEos2 [19], has overcome the temperature sensitivity, fluoresces ~30% more brightly than the other green-to-red photoconverters and displays a photostability that equals or betters all other PA-FPs.

Kaede [11] is another green-to-red highlighter, which is the brightest in the green state and roughly equivalent to the originally published EosFP variants. KikGR [12] was engineered from a non-photoactivatable FP based on the Kaede structure, but like Kaede is tetrameric and unsuitable for fusion protein studies because of the possibility of mistargeting/aggregation. Fortunately, a monomeric version of KikGR has recently been developed and has been successfully used in both diffraction-limited and super-resolution imaging [20]. Dendra2 [14], another green-to-red highlighter, is monomeric and gives a 4500-fold increase in the red-to-green ratio after photoconversion [14].

PS-CFP2 is a photoswitchable cyan FP that photoconverts from cyan to green upon irradiation at 405 nm [21]. The cyan fluorescence observed before photoconversion makes it easy to find regions for selective illumination. The green-to-cyan ratio after activation is >2000-fold, producing good contrast that is similar to the other photoconversion proteins. In addition, PS-CFP2 is monomeric so it is useful as a fusion protein tag. PS-CFP2 has been used in two-color, super-resolution experiments with EosFP because of its higher photon output than PA-GFP [8]. PS-CFP2 photon yield and its photoconversion into a green state with little red fluorescence should also make it a good partner with PAmCherry1 [7] or some of the other red PA-FPs discussed below.

Reversible highlighters

The third class of PA-FPs, reversible highlighters with on/off switching, includes FP595 [22], Dronpa [11] and its variants [23,24], red reversible PA-Cherry molecules (rsCherry and rsCherryRev) [25], Kindling-FP [26], IrisFP [27], DsRed timer [28] and monomeric blue-to-red timers [29]. These PA-FPs are characterized by their ability to be repeatedly photoconverted between two states using light of two distinct wavelengths. In the case of Dronpa, one of the better known reversible highlighters, it initially fluoresces green and is monomeric [30]. Prolonged or intense irradiation with 470–510 nm light causes switching to a non-fluorescent chromophore form. Dronpa can then be reversibly activated back to its green fluorescent form by irradiation at 400 nm light. This activation-quenching cycle can be repeated many times in a single cell expressing this protein. The large extinction coefficient and quantum yield of Dronpa make it the brightest of any PA-FP. However, in PALM experiments its photon yield does not match expectations [8]. This might be because 488 nm light both excites Dronpa's fluorescence and inactivates its chromophore, leading to the molecule switching off before emitting all of its potential photons. A variant of Dronpa, called Padron, displays the opposite photoswitching behavior and can overcome this potential problem by being activated with blue light and inactivated with UV light [24]. The rsCherry and rsCherryRev variants [25] are based on mCherry [31], which makes them monomeric. They have relatively high background fluorescence, but their single molecule brightness and photoswitching between darker and red states make them potential partners with several of the green PA-FPs. In the case of Kindling-FP [26], low intensity green or yellow light results in transient red fluorescence, termed kindling, which slowly decays back to a non-fluorescent state. Intense blue light can be used to immediately quench the red fluorescence, whereas high intensity green illumination results in irreversible photoconversion to the red state. The on/off switching capability of the reversible highlighters has been utilized in a variety of ways for the spatiotemporal tracking of molecules within cells.

Imaging with PA-FPs

Photoactivation usually requires a separate excitation source than the one used for imaging (with ~400 nm irradiation required in most cases). After photoactivation,

imaging is similar to that used for conventional FPs. An ideal PA-FP should be readily photoactivatable/photoconvertible to generate a high level of contrast. Nevertheless, the particular features of PA-FPs make them preferable for specific types of applications. For example, in experiments using a PA-FP-tagged fusion protein, monomeric PA-FPs are recommended to avoid protein aggregation artifacts. Long-term tracking experiments need PA-FPs with sufficient photostability after activation to be imaged for the duration of the experiment. In multi-label experiments, PA-FPs that have minimal spectral overlap are required. Finally, in super-resolution experiments, PA-FPs with high single molecule brightness and low background are best for mapping the distribution of the proteins with high precision.

Regardless of which PA-FPs are used in a particular application, efforts are needed to optimize conditions for imaging [32]. In the case of diffraction-limited imaging, levels of fluorescence post-photoactivation must be estimated to avoid detector saturation because fluorescence at the imaging wavelength after photoactivation increases dramatically. In addition, optimization of the amount of light used during photoactivation is needed to obtain the highest level of photoactivation with the least amount of irradiation and photobleaching of the sample. Efforts are further needed to ensure specific structures/areas can easily be photoactivated. This is particularly important when using dark-to-bright PA-FPs, such as PA-GFP. Locating a cell or specific region of a cell to activate can be difficult using dark-to-bright PA-FPs because the molecules have little fluorescence before photoactivation. Cells can be cotransfected with a second red or cyan FP to reveal positive cells or structures. Green-to-red and cyan-to-green PA-FPs avoid this problem because the pre-activated emission wavelength can be used to target the activation laser.

The poor axial (z) resolution of conventional, diffraction-limited imaging makes it difficult to spatially confine the photoactivation process in the axial dimension. Two-photon activation of PA-FPs overcomes this problem by activating subfemtoliter volumes, providing unique control of photoactivation in 3D space [33–35]. Moreover, because this approach greatly minimizes photoactivation in the axial dimension, the potential for phototoxicity in whole animal imaging is decreased. These properties make two-photon photoactivation a unique tool for many cell and developmental biology applications. The next few sections provide examples of these applications and the biological insights they have revealed.

PA-FP applications in conventional diffraction-limited imaging

Tracking cellular compartments and structures

Most biological structures within cells are part of larger steady-state systems, in which input and outflow pathways continuously circulate components. Insight into these pathways, a requirement for understanding how the structure can maintain itself, is often impossible using conventional FP imaging. This is because the ensemble of visible FP fusion proteins in a compartment is at steady state, with signal gain balanced by signal loss. PA-FPs offer a powerful approach for dissecting protein trafficking patterns and inter-organelle exchange within such steady-state systems because discrete populations of proteins in the system can be selectively highlighted and followed over time. This is illustrated in Figure 1, in which PA-GFP-tagged molecules moving through the secretory pathway are 'switched on' by photoactivation selectively in the Golgi apparatus – the central sorting and processing station of the secretory pathway. Photoactivated cargo molecules can be seen quickly exiting the Golgi moving outward along curvilinear tracks in small vesicles that later fuse with the plasma membrane (PM). This type of photoactivation-chase (photo-chase) approach has been used to study the dynamic properties of other membrane organelles and cytoskeletal structures within cells, as discussed in the examples below.

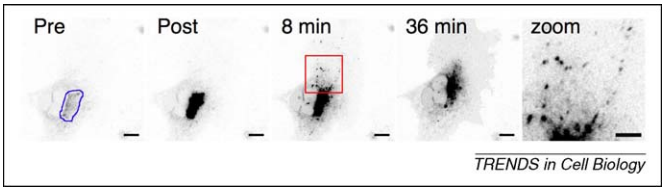

Figure 1. Photolabeling of a Golgi pool of PA-GFP-tagged VSVGtsO45. A COS-7 cell expressing a temperature sensitive VSVGtsO45-PA-GFP was transfected and incubated overnight at the non-permissive temperature of ~40 °C. This accumulated the protein in the ER because of the misfolding of the VSVGtsO45. After shifting to the permissive temperature of 32 °C on the microscope stage for ~40 minutes, which releases VSVGtsO45-PA-GFP into the secretory pathway, the Golgi pool of the protein (indicated in the outline in the pre-photoactivation image) was photoactivated with ~400 nm light. Photoactivation resulted in a brighter pool of molecules in the Golgi area (post) that moved from the Golgi to the PM (8 and 36 min). Scale bars are 10 μm. The zoomed view of the 8 min time point shows transport carriers moving from the Golgi apparatus to the PM. Scale bar is 5 μm in the zoom image.

Use of photo-chase experiments have made it possible to address whether lysosomes actively communicate with each other or are dead-end structures [5]. After photoactivating PA-FP-tagged lysosomal membrane components in a subset of lysosomes, the signal seemed to disperse throughout the cell within 15 minutes in most lysosomes. This occurred through tubular/vesicular carriers that conveyed the photoactivated molecules from one lysosome to another in a microtubule-dependent manner. Therefore, individual lysosomes within a cell dynamically communicate with other lysosomes/endosomes through membrane transport pathways.

The origin of peroxisomes, which metabolize fatty acids and peroxides, has also been addressed in photo-chase experiments [36]. PEX16p-PA-GFP, an early event peroxisomal protein in mammalian cells, was selectively photoactivated in the endoplasmic reticulum (ER). The highlighted molecules were found to move from the ER to peroxisomes over time, supporting an ER origin of peroxisomes. In other photo-chase experiments, peroxisomes were found to proliferate primarily by outgrowth from the ER rather than by division. This was demonstrated by photoactivating all peroxisomes at time zero, culturing for a number of hours and then photoactivating cells a second time. A comparison of the photoactivation patterns directly before and after the second photoactivation step revealed that the new peroxisomes did not contain previously photoactivated molecules. This ruled out peroxisome proliferation by division, which predicts that any new peroxisomes should contain old material.

Photoactivation-based experiments have also been used to address the dynamic characteristics of other

membrane-bound organelles. In a study examining the dynamics of mitochondria, Wiedenmann et al. [13] highlighted a subregion of mitochondrial network using a EosFP-tagged mitochondrial-targeting signal and then examined how quickly the signal transferred to other mitochondrial elements. Transfer depended on the dynamic fusion and fission activities of mitochondria. In a different study, Hailey et al. examined the turnover rate of autophagosomes by switching on an entire population of autophagosomes labeled with PA-GFP-LC3 in starved cells [37]. After highlighting the autophagosomes, the signal was lost with a half-time of ~30 min, revealing the remarkably fast turnover of these organelles. Another study used PA-FPs to examine plant plasmodesmata, the narrow bridges that connect different plant cells with each other [38]. The selective photoactivation of molecules in one plant cell resulted in the unidirectional transport of the highlighted molecules through plasmodesmata to neighboring cells.

Structures comprising the cytoskeleton have also been dissected by photoactivation experiments. Using a mammalian cell line expressing PA-GFP-tubulin, Ferenz and Wadsworth [39] highlighted tubulin molecules within mitotic spindle arrays. Photoactivated marks moved toward and away from spindle poles at a wide range of rates. The variability of this motion decreased as mitosis progressed with only slow, poleward-directed motion remaining at metaphase. This resulted from the progressive changes in microtubule organization during spindle formation rather than changes in mitotic motor activity, a key finding for understanding the mechanics of mitotic spindle arrays.

Selective photoactivation strategies have been used to visualize actin treadmilling along individual filaments [18], as well as intermediate filament assembly [40]. In the case of intermediate filament assembly, highlighted vimentin PA-FPs incorporated along the entire length of intermediate filaments rather than adding only at the filament ends, as occurs for microtubule and actin remodeling. The intermediate filaments were further found to remodel by end-to-end annealing of assembled filaments.

The use of photoactivation technology to create transients in a steady-state population of molecules promises to answer many more questions regarding how organelles and structures assemble, remodel and turn over in living cells.

Tracking cells in tissues and embryos

PA-FPs have widespread utility for the study of early development. In one approach, capped mRNA coding for tdEosFP was injected into frog embryos at the two-cell stage and resulted in green embryos [41]. This permitted the researchers to study coordinated cell movement during embryonic development because subsets of cells could be photoconverted and their movement followed over time. Localized photoconversion and following the photoconverted cells in this manner permitted the analysis of cell movement for up to nine days. Among the processes studied with this approach were cell monolayer rearrangements during convergence and the extension of the neural epithelium. In a related approach, Kaede cDNA linked to the 3′ untranslated region (UTR) of β-actin was injected into cells fated to become the retina by injection into frog blastomeres. The rate of transgene expression in the retinal growth cone was then measured [42].

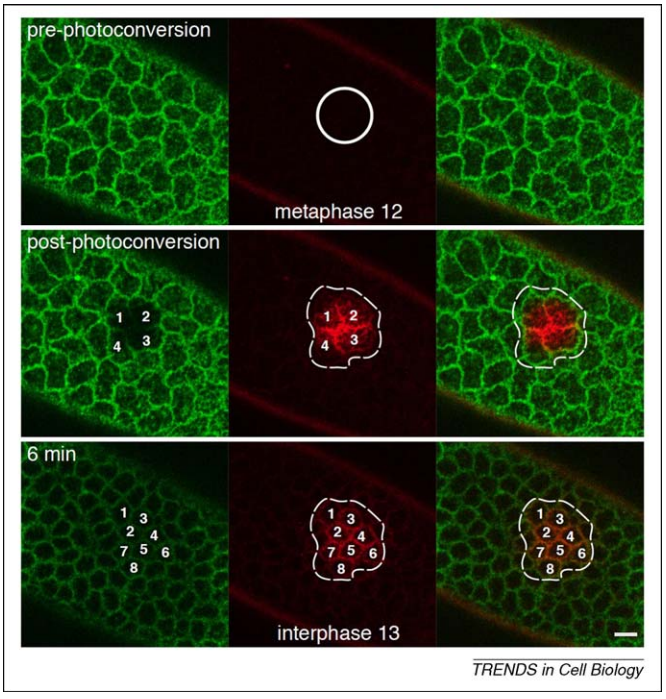

Figure 2. Optical pulse-chase labeling of the PM marker GAP43 fused to EosFP during syncytial divisions in a fly embryo. The data reveal that activated GAP43 fluorescence stays associated with PM regions neighboring individual nuclei and its daughters over time instead of spreading more widely across the PM surface of the embryo. Figure from [43].

In another study, Mavrakis et al. [43] imaged fly embryos expressing a PM protein tagged with tdEosFP. By selectively highlighting a subset of molecules on the PM in the early syncytial blastoderm embryo, they found that the PM is compartmentalized around each of the multitude of nuclei (Figure 2). Molecules diffuse within domains above each nucleus, but do not exchange between PM regions of adjacent nuclei. Furthermore, drug-induced F-actin depolymerization disrupts the diffusion barriers within the syncytial PM. The PM compartmentalization within early embryos discovered using these techniques could serve to shape morphogen gradients before cellularization, with important implications for early fly embryo organization and development [43].

Protein diffusion and binding kinetics

Binding and dissociation kinetics play key roles in determining how proteins associate at steady state within protein complexes or structures. Although fluorescence recovery after photobleaching (FRAP) originally was employed to gain insight into rates of binding and dissociation, this approach cannot easily estimate off rates without requiring additional information on total pools of molecules. PA-FPs offer a powerful addition to FRAP for the analysis of the kinetic properties of proteins at the subcellular level (Figure 3); rather than removing a subpopulation from view as in photobleaching, photoactivation permits the direct highlighting of subpopulations to follow their movement. By combining FRAP and photoactivation, as discussed below, researchers have made great progress in clarifying protein dynamics within cells.

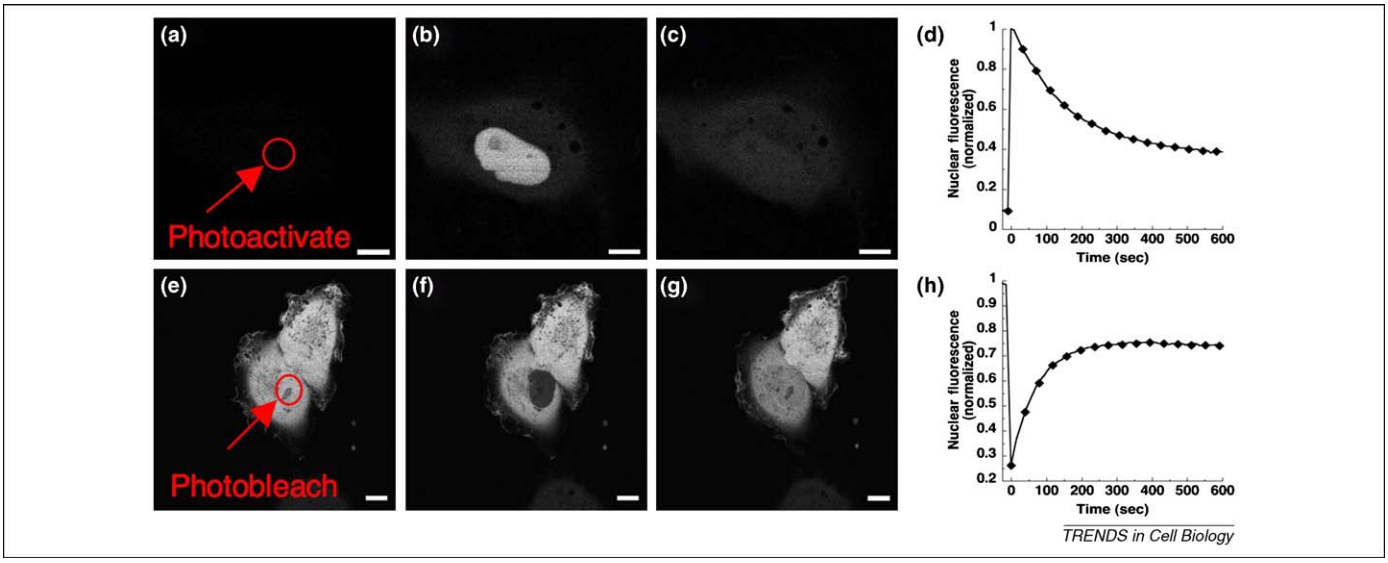

Figure 3. Photoactivation and photobleaching of untagged fluorescent proteins. COS-7 cells expressing PA-GFP **(a–d)** were photoactivated in the nucleus indicated by the red circle and followed as the nuclear fluorescence signal equilibrated with the cytoplasm. Photoactivated fluorescence signals, such as the nuclear pool **(d)**, can be quantified and used to study the kinetics of molecular movement out of the nucleus in this example. Here, the data are normalized to the first post-activation image. For comparison, the nuclear pool in COS-7 cells expressing EGFP **(e–h)** were photobleached (indicated by the red circle in E) and followed as the fluorescent molecules in the cytoplasm equilibrate with the nucleus. This technique, often called FRAP (fluorescence recovery after photobleaching), is complimentary to photoactivation experiments and used to study the kinetics of molecular movement, such as the movement of EGFP into the nucleus in this example. The graph in H shows the nuclear signal during this FRAP experiment and is normalized to the pre-photobleached image. Scale bars are 10 μm.

Early endosomal antigen 1 (EEA1) is a cytosolic protein that by binding to early endosomes helps tether them together before homotypic endosome–endosome fusion. To gain insight into how EEA1 binding is fine-tuned to control the tethering and fusion of early endosomes, Bergeland et al. used FRAP and photoactivation to examine the binding/dissociation kinetics of EEA1 tagged with PA-GFP or GFP [44]. Their results revealed that EEA1 only transiently associates with endosomes before dissociating again into the cytoplasm with its off rate modulated for tuning of various functions.

In a different study, Deryusheva and Gall used photoactivation to examine the properties of Cajal bodies (CBs) – subnuclear organelles involved in RNA transcription and processing [45]. Coilin, a major component of CBs, was labeled with PA-GFP and its movement analyzed in unfixed, isolated nuclei. PA-GFP-coilin exited from CBs into surrounding nucleoplasm in minutes and diffused very slowly within CBs. The movements were unaffected by the transcriptional state of the nucleus or ongoing nucleocytoplasmic exchange. Thus, the data suggested that CB components are in a constant state of flux and are likely to be undergoing reversible assembly into large complexes within a CB.

PA-FP-based approaches have also been used to investigate the dynamics of Smad proteins, which transduce signals from the transforming growth factor β (TGFβ) receptor at the PM to the nucleus. This occurs by Smad translocation into the nucleus and binding to gene regulatory components. To understand the dynamics of this process, Schmierer and Hill used a combined FRAP and photoactivation strategy, quantifying Smad2 nucleocytoplasmic shuttling [46]. They found that Smad2 underwent continuous, rapid shuttling into and out of the nucleus. In response to TGF-1 receptor binding, Smad2 accumulated in the nucleus through a process involving the inhibition of its nuclear mobility and export rate. The data revealed the TGF-1-dependent nuclear accumulation of Smad2 occurs by selective nuclear trapping of complexed Smad2.

Protein–protein interactions

PA-FPs have begun to be used to study protein–protein interactions with fluorescence resonance energy transfer (FRET) techniques. FRET involves the nonradiative transfer of energy from a donor fluorophore to an acceptor fluorophore that are in close proximity. A promising PA-FP-based FRET approach, called photoquenching FRET (PQ-FRET), uses photoactivated PA-GFP as an acceptor to quench the fluorescence of a donor fluorophore, such as cyan fluorescence protein (CFP) [47]. Demarco et al. used PQ-FRET to monitor the interactions of a heterochromatin protein and a transcription factor within distinct domains of the nuclei of living cells. Variations of PQ-FRET should be possible with other FRET pairs, such as CFP and Dronpa. Proximity of tagged proteins would be signaled when the intensity, or lifetime, of CFP fluorescence (acting as the FRET-pair donor) was affected by Dronpa photoswitching (acting as the FRET-pair acceptor).

PA-FP applications in single molecule super-resolution imaging

PA-FPs have become valuable tools in new super-resolution microscopy techniques that overcome the diffraction barrier [17,48,49]. These techniques permit biologists to visualize the structures and processes of the cell at the molecular level. Key among these super-resolution techniques employing PA-FPs are photoactivated localization microscopy (PALM) [17] and fluorescence photoactivation localization microscopy (F-PALM) [48], herein both referred to as PALM. Another variation of a molecular localization technique, called stochastic optical reconstruction microscopy (STORM) [50], uses reversibly switching Cy3–Cy5 pairs, instead of PA-FPs, to assemble images.

PALM/STORM involves imaging of PA-FP or switching cyanine molecules individually and then localizing them to high precision by determining their centers of fluorescence emission (Figure 4). Low-level illumination is used to photoactivate individual molecules spaced far enough apart that their diffraction-limited spots, recorded on a highly sensitive camera, do not overlap. The photon distributions within each spot, whose dimensions are defined by the microscope's point spread function (PSF), are then statistically fit to determine their centroids, down to 10 nm optical precision. Repeating this process reveals the precise localization of a new group of molecules. By rendering each fitted molecule in all frames as two-dimensional Gaussian distributions centered at the determined coordinates, a super-resolution image is obtained. Imaging is often performed with total internal reflection fluorescence (TIRF) microscopy to minimize background fluorescence and with an electron-multiplying charge coupled device (EMCCD) camera to optimally detect single molecules.

Super-resolution approaches employing single molecule localization such as PALM/STORM are rapidly progressing [51,52]. They have opened the door for looking at the organization and dynamics of protein ensembles within cellular structures and membranes, and quantifying spatial correlations of proteins within such ensembles. As such, they hold great promise for biological imaging at unprecedented resolution.

Structural PALM

Structural PALM imaging, using fixed cells, has revealed molecular distributions of PA-FPs in subcellular structures at very high densities ($>10^5$ molecules per μm^2) [17]. Either fixed whole cells or cryosections of cells on coverslips can be imaged in this approach. One consideration for such experiments is the use of fixatives on the cells. In some cases, PA-FPs can lose fluorescence, especially when using glutaraldehyde. And, with the molecular precisions capable with these new techniques, the continuing debate within the electron microscopy community regarding ultrastructural changes caused by chemical fixatives versus cryofixation becomes relevant.

In whole cells, the molecular details of proteins within structures at nanometer resolution have been revealed. These include vinculin at focal adhesion sites, actin within stress fibers and proteins embedded within the PM [8,17,53]. In addition to biological structures, PALM imaging has provided new insights into the spatial organization of signaling networks within cells. Greenfield et al. used structural PALM imaging to analyze sensory clusters comprising the *E. coli* chemotaxis network [54]. By mapping at 15 nm resolution clusters of three proteins comprising sensory clusters, the authors showed that cluster formation occurred via stochastic self-assembly without cytoskeletal involvement or the active transport of components.

To view intracellular structures expressing PA-FPs deep within whole cells, thin cryosections [as used in transmission electron microscopy (TEM)] can be imaged by PALM. This has permitted the visualization of the molecular distributions of proteins within lysosomes, endosomes, Golgi apparatus and mitochondria [17]. An advantage of PALM imaging of cryosections, besides their low background fluorescence, is that they can be imaged by TEM after PALM. In such a correlative PALM/TEM imaging approach, cryosections on EM grids are first imaged using

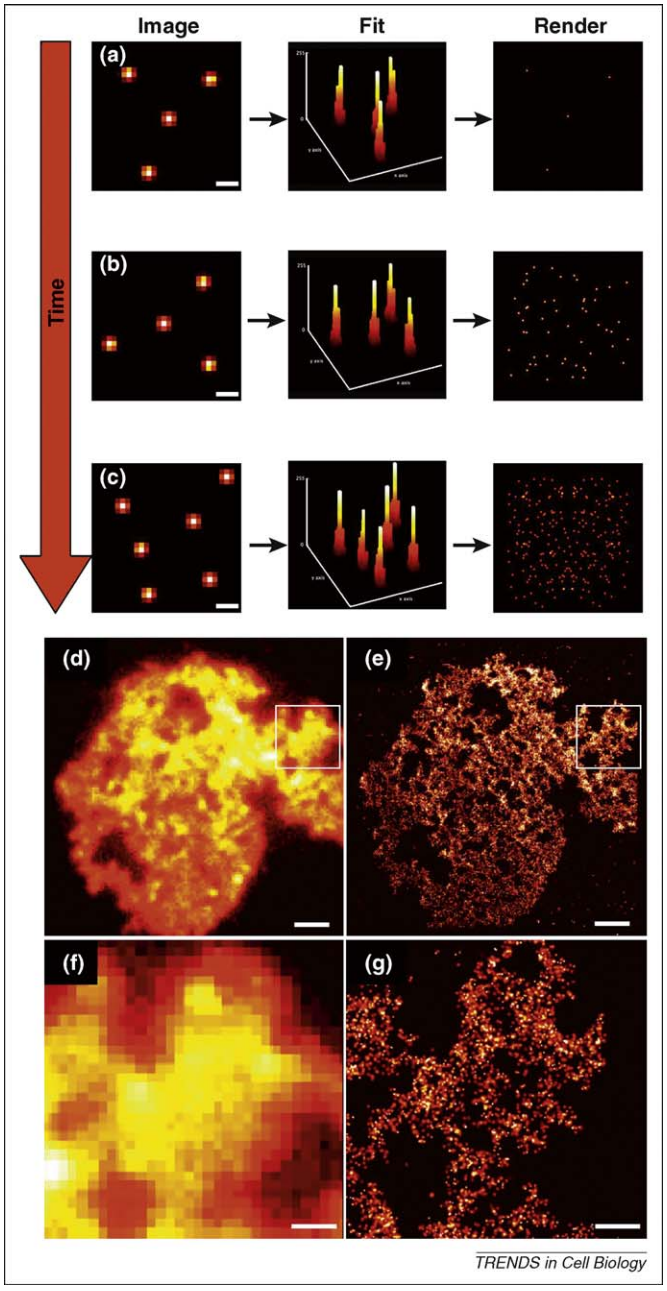

Figure 4. Principle of high-density molecular localization achieved by techniques such as PALM, F-PALM and STORM. Techniques falling into this class of imaging are single molecule imaging methods, but the key is to make possible the imaging of single molecules in a field containing hundreds or thousands **(a–c)**. Molecules of interest tagged with fluorescent proteins or other labels that are initially dark and can be photoactivated or switched to a non-fluorescent state are 'turned on' in small numbers to maintain a density low enough to distinguish single molecules. Each molecule is precisely localized by a 2D Gaussian fit of the photon distribution rendered in a new image as a Gaussian distribution using the determined x, y coordinates and a size indicated by the uncertainty of fit of the original photon distribution. The photoactivation and imaging of all the molecules within a specimen and summing the diffraction-limited fluorescence results in an image that is equivalent to a conventional optical image **(d)**. But, rendering all of the localized molecules on the same image gives a super-resolution image for these simulated molecules of interest **(e)**. Zoomed images **(f)** and **(g)** better demonstrate the level of detail available in the PALM image **(g)** compared with the conventional image **(f)**. Scale bars in **(a–c)** are 0.5 μm. Scale bars are 2 μm in **(d)** and **(e)** and 0.5 μm in **(f)** and **(g)**. **(d–g)** are reprinted from [17].

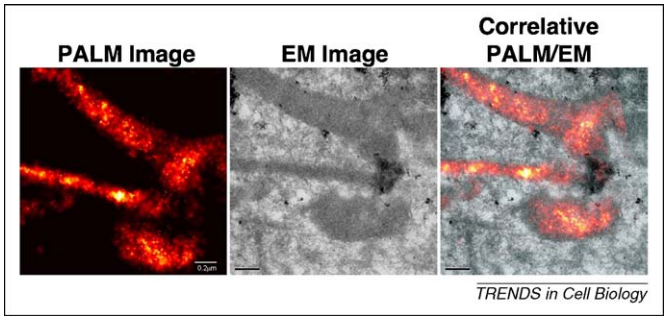

Figure 5. Correlative PALM/EM images of mitochondria in a cryoprepared thin section from a COS-7 cell expressing a dEosFP-tagged cytochrome *c* oxidase import sequence. Reprinted from [17].

PALM. The grids are then gently removed from the PALM microscope and transferred to the transmission electron microscope for imaging. This approach provides a high-density alternative to immunogold labeling, with over 5500 molecules associated with a subset of mitochondria in a single cryosection [17] (Figure 5). In comparative immunogold experiments, by contrast, only ~10–20 molecules are typically observed. One of the most valuable features of correlative PALM/TEM is that it provides the needed nanometer-scale resolution of cell ultrastructure to correlate with PALM images, which is crucial to ensuring novel results are accurate.

An additional promising approach for PALM viewing deep within cells or tissues is based on combining the lateral super-resolution provided by PALM with two-photon temporal focusing and optical sectioning [35]. Thin layers of samples (~1.9 μm) are successively excited using two-photon irradiation and then imaged using PALM. The layers are then combined to produce a volume image several micrometers in depth. This approach has successfully generated super-resolution images of mitochondria and PM over an axial range of ~10 μm. Whereas PALM combined with two-photon microscopy allows imaging deep within samples, the z resolution of its images are still diffraction-limited (~500 nm), limiting its use in the 3D characterization of cellular super-structures.

Multicolor PALM

Two-color PALM using different pairs of PA-FPs, which allows more than one labeled protein in the same specimen to be visualized, is now possible. As such, it offers enormous opportunities for dissecting the organization of protein ensembles in the membrane and quantifying spatial correlations between different classes of proteins.

Several strategies have been used to perform two-color PALM [7,8,10]. In one approach, endogenously expressed PA-FP pairs, either Dronpa/EosFP or PS-CFP2/EosFP, are used [8]. A specimen expressing these pairs is initially exposed to UV light, and then a 561 nm EosFP excitation light is used until all EosFP molecules are detected, localized and bleached. The Dronpa molecules are then deactivated using an intense 488 nm light before they are reactivated, detected and localized. Summed images are combined from both partners to construct the final double-label image. The main drawback of this approach is that the partner molecules need to be imaged sequentially rather than simultaneously. Moreover, for Dronpa paired with tdEosFP, photoswitching of the fluorophores between light and dark states is required, potentially complicating results. This problem also applies to the two-color scheme used in PALMIRA [10], in which photoswitchable rsFastlime is paired with Cy5. This restricts these approaches for use in fixed cells.

A more recent two-color PALM strategy, employing PA-GFP and PAmCherry1 [7], does not have these drawbacks. This is because the respective red and green wavelengths of PAmCherry1 and PA-GFP do not overlap. In this approach, PA-GFP and PAmCherr1y are both switched on with UV light, and a 488 nm PA-GFP excitation light and 561 nm PAmCherry1 excitation light is then used to detect, localize and bleach the molecules simultaneously. Two-color PALM employing PA-GFP and PAmCherry1 has been used to map out the nanomeric distribution of transferrin receptor and clathrin in clathrin-coated structures at the PM [7]. The lack of spectral overlap of the PA-GFP and PAmCherry1 make the use of this pair more straightforward than the previously described techniques, but results in a loss in localization precision in the green channel because of the higher background signal of PA-GFP. However, this approach can also be used with several of the other green PA-FPs mentioned earlier. In fact, given the higher contrast of Dronpa, Dronpa derivatives and PS-CFP2, these should result in even better precision when employed as partners with PAmCherry1.

3D super-resolution imaging

Because the axial (z) resolution is significantly poorer than the x-y resolution in diffraction-limited imaging, improvements in z resolution have been a major focus in microscopy development for super-resolution imaging [55–58]. The most promising for use in single molecule localization techniques, such as PALM and STORM, include strategies employing defocusing [56,57], double helix PSF (DH-PSF) imaging [59] and interferometry [60].

One defocusing approach for 3D super-resolution imaging [56] employs a cylindrical lens in the imaging optics to shift the focus in x and y directions, making the image from single molecules elliptical. The center of the ellipsoid is then fit, providing improved z resolution. This strategy has achieved an x-y resolution of ~25 nm and z resolution of ~50-nm with photoswitchable cyanine dyes. A second defocusing approach splits the emission light so that each follows different path lengths [57]. Defocusing the shape of the resulting single molecule image allows for the determination of the z coordinate. An axial localization precision of 75 nm has been achieved with caged fluorophores using this approach. An attractive feature of both these defocusing approaches is that by scanning in the z plane several micron thick specimens can be analyzed.

The DH-PSF and interferometry super-resolution imaging approaches have achieved sub-20 nm resolution, providing the best 3D spatial resolution for single molecule localization imaging to date. DH-PSF imaging achieves 3D resolution using a microscope whose PSF has been engineered to produce two lobes, which are rotated with respect to the image depending on their axial position within the focal plane [59]. This enables 20 nm axial resolution over z ranges of >2 μm. Interferometry super-resolution imaging

integrates a single-photon multiphase interferometric scheme with PALM [60]. This approach is called interferometric photoactivated localization microscopy (iPALM). Specifically, a single photon derived from a photon emitter (i.e. PA-FP), after traveling different path lengths dependent on the axial position of the emitter, is allowed to self-interfere in a three-way beam splitter. The three output beams from the splitter are then used to determine the axial position of the source molecule, whose x-y position is determined via PALM.

iPALM provides a 10-fold improvement in axial resolution and a 100-fold improvement in photon efficiency compared with defocusing techniques [60]. This makes it particularly suited for accurate 3D localization of PA-FPs, whose modest photon output (usually one-tenth that given off by cyanine dyes) limit their usefulness in 3D imaging using defocusing. Figure 6 provides an example of an iPALM image of farnesylated proteins on the PM, in which individual molecules are color-coded according to their axial position (with red molecules closest and purple molecules most distant from the bottom of the cell). iPALM imaging has resolved the diameter of microtubules to nearly their known dimension of 25 nm along the z-axis. In addition, the dorsal and ventral positions at the leading edge of the PM (~50 nm distance) could be distinguished, and the 3D organization of α_v integrin within focal adhesions [60]. The sub-20 nm, 3D spatial resolution capability of iPALM, which should soon be applicable to multi-color approaches and single particle tracking, has much potential for the quantitative measurement of protein distributions and topologies that underlie the complex, molecular-scale structures found within cells.

Live cell PALM

Extending PALM to living cells has recently become possible because of improvements in PALM imaging collection rate, excitation power and probe brightness. Hess et al. and Shroff et al. were the first to demonstrate live cell PALM by following different molecules associated with the PM [53,61]. More recently, Biteen et al. performed time-lapse imaging of single bacterial actin proteins in *Caulobacter crescentus* cells [62]. Hess et al. examined hemagglutinin (HA) molecules from the influenza virus and analyzed their behavior within clusters distributed across the PM. By contrast, Shroff et al. followed individual adhesion complexes. They captured many super-resolution images of adhesion complexes labeled with tdEosFP-paxillin at 25–60 s time intervals from a single living cell. Because enough molecules were localized per frame to resolve adhesion complexes, and during each frame adhesion complexes moved slowly, it was possible to characterize how these structures evolved over time. The data revealed significant spatiotemporal changes in the nanoscale organization of adhesion complexes that would have been undetectable by conventional diffraction-limited imaging. For example, different zones of an individual adhesion complex moved at variable rates, recruited or lost different overall numbers of molecules, and underwent different shape changes. Although the PALM frame rate of 25–60 s was sufficient to study adhesion complex dynamics, it is clearly inadequate for studying cellular processes occurring on a faster timescale. For this, faster imaging will be required, but how fast remains open for debate. Given the current palette of PA-FPs and available excitation powers for increasing the

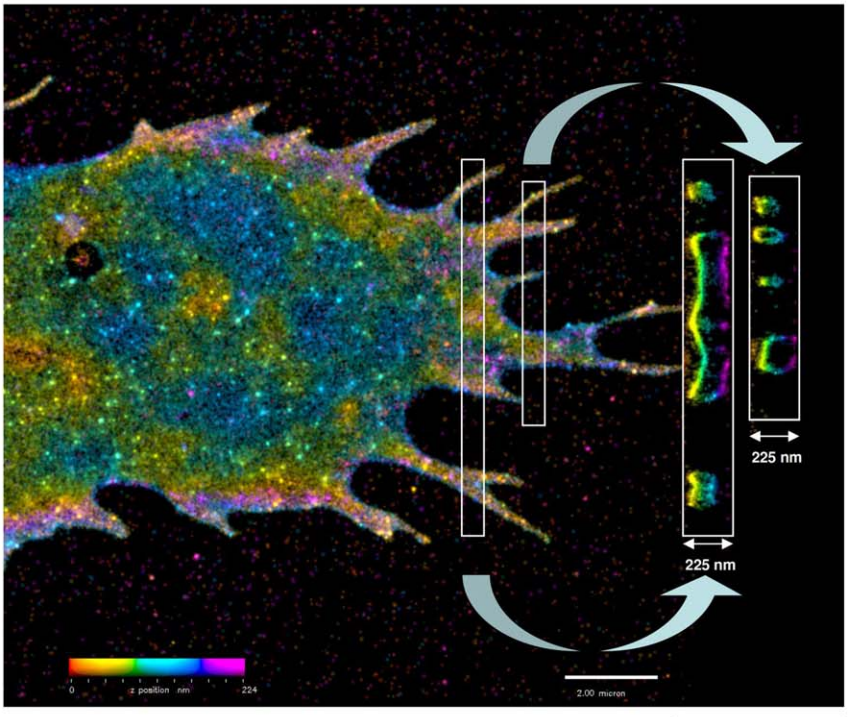

Figure 6. Super-resolution iPALM image of a FoLu cell expressing farnesylated tdEosFP at the PM, rendered with z-axis color-coding. The areas outlined in white are shown as a z cross-section. Image was kindly provided by Harald Hess and Gleb Shtengel, Janelia Farm Research Campus, Ashburn, VA, USA.

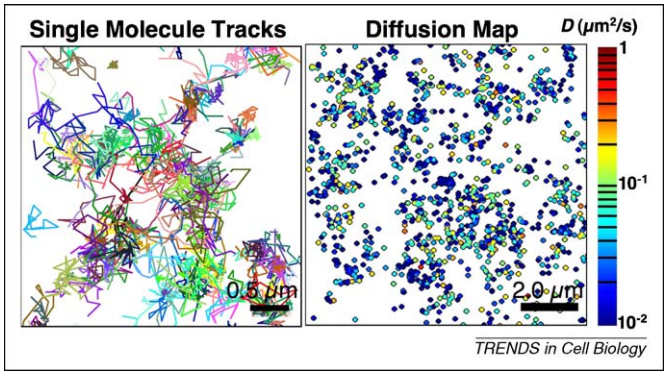

Figure 7. SptPALM imaging of the ts045 vesicular stomatitis virus G protein tagged with Eos (VSVG) expressed in live COS-7 cells. Left panel shows the summed trajectories of localized VSVG-Eos molecules. Each color represents a different track, all of which were longer than 15 frames at a 50 ms/frame rate (scale bar = 0.5 μm). Right panel shows a diffusion map of VSVG-Eos expressing cells. Each point represents the starting position of one trajectory and is color-coded according to the diffusion coefficient (D_{eff}) calculated for the trajectory (see color lookup table on right for values of D_{eff}) (scale bar = 2.0 μm). Reprinted from [63].

number of molecules localized per unit area per unit time, it is possible that rates of 2–10 s at resolutions of 50 nm might eventually be achieved [61].

Single particle tracking PALM

PALM has been combined with single particle tracking to provide information on the dynamics of individual PA-FP-tagged molecules in live cells [63,64] (Figure 7). Unlike traditional single particle tracking in which a single ensemble of molecules is imaged and tracked until they are bleached, single particle tracking PALM (sptPALM) involves continuous low light activation so that over long periods numerous molecules can be switched on and tracked until photobleached. Because of the low level activation light, the distance between fluorescent molecules switched on at any time is nearly always greater than several times the width of their PSF. Hence, molecules in each frame (~50 ms) can be fitted to high precision and their trajectories over successive frames mapped. This permits the collection of high-density spatial maps of up to 50 tracks per μm^2, many of them overlapping, over many minutes of imaging.

Using sptPALM, Manley et al. [63] compared the distribution and dynamics of two PA-FP-tagged viral proteins expressed in the PM, the ts045 vesicular stomatitis viral G protein (VSVG) and the HIV type 1 (HIV-1) structural protein Gag. Spatially resolved maps of single molecule diffusion coefficients of these proteins revealed strikingly different diffusional behavior; whereas VSVG molecules were highly mobile and freely explored the PM (Figure 7), Gag proteins were often in immobile clusters approximating the size of viral-like particles (~100–200 nm diameter).

sptPALM has also been used to investigate the dynamics of FtsZ, the bacterial homolog of tubulin that forms a helical filamentous structure (i.e. Z-ring) important for bacterial cytokinesis [64]. FtsZ-Dendra2 proteins imaged in *E. coli* using sptPALM revealed both stationary and mobile molecules. Interestingly, FtsZ-Dendra2 molecules associated with the Z-ring appeared stationary even though FRAP studies previously demonstrated the Z-ring was a highly dynamic structure. This suggested that remodeling FtsZ molecules in Z-rings occurs by local binding and dissociation rather than by active transport or treadmilling behavior.

Concluding remarks

PA-FPs and their associated emerging techniques are heralding a new era in cell biology. These genetically expressed FPs permit the non-perturbative optical imaging of dynamic processes in living cells. For a cell biologist interested in using photoactivation or even super-resolution experiments, the large number of possible probes can seem overwhelming. Many PA-FPs have contributed to the cell biology community over several years. Many of these have been cited throughout this review and provide an excellent guide to which proteins work well for the purposes of the individual biologist. But as with any technology, improvements are continuously making their way out of the development stages and these certainly offer advantages over the previous generations of PA-FPs. One that should be considered is the mEos2 from McKinney and colleagues [19]. This is one of the brightest PA-FPs, being second only to Dronpa and ~30% brighter than the other green-to-red versions, and it has the photostability comparable with or better than most other PA-FPs. Another recent addition is PAmCherry1 [7], which is based on mCherry. It lacks the brightness and photostability of the mEos2, but is the brightest of the red PA-FPs that switch from off to red. Thus, its lack of a green fluorescent component makes it a good partner for green PA-FPs, such as PA-GFP, PS-CFP2 and Dronpa. Although most evidence is either unpublished or anecdotal, it seems that some PA-FPs work far better in some systems than in others and it would be unfortunate if an investigator decided to abandon photoactivation experiments based on a single failed attempt.

The various imaging approaches employing PA-FPs described in this review, both diffraction-limited and super-resolution, are only the beginning of numerous new possibilities to come. Further development of probes and instrumentation will certainly aid this process. But right now, researchers have before them a rich array of approaches to address many open biological questions.

References

1 Tsien, R.Y. (1998) The green fluorescent protein. *Ann. Rev. Biochem.* 67, 509–544
2 Lukyanov, K.A. *et al.* (2005) Innovation: photoactivatable fluorescent proteins. *Nat. Rev. Mol. Cell Biol.* 6, 885–891
3 Lippincott-Schwartz, J. and Patterson, G.H. (2008) Fluorescent proteins for photoactivation experiments. *Methods Cell Biol.* 85, 45–61
4 Fernandez-Suarez, M. and Ting, A.Y. (2008) Fluorescent probes for super-resolution imaging in living cells. *Nat. Rev. Mol. Cell Biol.* 9, 929–943
5 Patterson, G.H. and Lippincott-Schwartz, J. (2002) A photoactivatable GFP for selective photolabeling of proteins and cells. *Science* 297, 1873–1877
6 Verkhusha, V.V. and Sorkin, A. (2005) Conversion of the monomeric red fluorescent protein into a photoactivatable probe. *Chem. Biol.* 12, 279–285
7 Subach, F.V. *et al.* (2009) Photoactivatable mCherry for high-resolution two-color fluorescence microscopy. *Nat. Methods* 6, 153–159
8 Shroff, H. *et al.* (2007) Dual-color super-resolution imaging of genetically expressed probes within individual adhesion complexes. *Proc. Natl. Acad. Sci. U. S. A.* 104, 20308–20313
9 Habuchi, S. *et al.* (2005) Reversible single molecule photoswitching in the GFP-like fluorescent protein Dronpa. *Proc. Natl. Acad. Sci. U. S. A.* 102, 9511–9516

10 Bock, H. *et al.* (2007) Two-color far-field fluorescence nanoscopy based on photoswitchable emitters. *Appl. Phys. B.* 88, 161–165
11 Ando, R. *et al.* (2002) An optical marker based on the UV-induced green-to-red photoconversion of a fluorescent protein. *Proc. Natl. Acad. Sci. U. S. A.* 99, 12651–12656
12 Tsutsui, H. *et al.* (2005) Semi-rational engineering of a coral fluorescent protein into an efficient highlighter. *EMBO Rep.* 6, 233–238
13 Wiedenmann, J. *et al.* (2004) EosFP, a fluorescent marker protein with UV-inducible green-to-red fluorescence conversion. *Proc. Natl. Acad. Sci. U. S. A.* 101, 15905–15910
14 Gurskaya, N.G. *et al.* (2006) Engineering of a monomeric green-to-red photoactivatable fluorescent protein induced by blue light. *Nat. Biotechnol.* 24, 461–465
15 Mizuno, H. *et al.* (2003) Photo-induced peptide cleavage in the green-to-red conversion of a fluorescent protein. *Mol. Cell* 12, 1051–1058
16 Nienhaus, K. *et al.* (2005) Structural basis for photo-induced protein cleavage and green-to-red conversion of fluorescent protein EosFP. *Proc. Natl. Acad. Sci. U. S. A.* 102, 9156–9159
17 Betzig, E. *et al.* (2006) Imaging intracellular fluorescent proteins at nanometer resolution. *Science* 313, 1642–1645
18 Wiedenmann, J. and Nienhaus, G.U. (2006) Live cell imaging with EosFP and other photoactivatable marker proteins of the GFP family. *Expert Rev. Proteomics* 3, 361–374
19 McKinney, S.A. *et al.* (2009) A bright and photostable photoconvertible fluorescent protein. *Nat. Methods* 6, 131–133
20 Habuchi, S. *et al.* (2008) mKikGR, a monomeric photoswitchable fluorescent protein. *PLoS One* 3, e3944
21 Chudakov, D.M. *et al.* (2004) Photoswitchable cyan fluorescent protein for protein tracking. *Nat. Biotechnol.* 22, 1435–1439
22 Lukyanov, K.A. *et al.* (2000) Natural animal coloration can be determined by a non-fluorescent green fluorescent protein homolog. *J. Biol. Chem.* 275, 25879–25882
23 Stiel, A.C. *et al.* (2007) 1.8 A bright-state structure of the reversibly switchable fluorescent protein Dronpa guides the generation of fast switching variants. *Biochem. J.* 402, 35–42
24 Andresen, M. *et al.* (2008) Photoswitchable fluorescent proteins enable monochromatic multi-label imaging and dual-color fluorescence nanoscopy. *Nat. Biotechnol.* 26, 1035–1040
25 Stiel, A.C. *et al.* (2008) Generation of monomeric reversibly switchable red fluorescent proteins for far-field fluorescence nanoscopy. *Biophys J.* 95, 2989–2997
26 Chudakov, D.M. *et al.* (2003) Kindling fluorescent proteins for precise *in vivo* photolabeling. *Nat. Biotechnol.* 21, 191–194
27 Adam, V. *et al.* (2008) Structural characterization of IrisFP, an optical highlighter undergoing multiple photo-induced transformations. *Proc. Natl. Acad. Sci. U. S. A.* 105, 18343–18348
28 Terskikh, A. *et al.* (2000) "Fluorescent timer" protein that changes color with time. *Science* 290, 1585–1588
29 Subach, F.V. *et al.* (2009) Monomeric fluorescent timers that change color from blue to red report on cellular trafficking. *Nat. Chem. Biol.* 5, 118–126
30 Ando, R. *et al.* (2004) Regulated fast nucleocytoplasmic shuttling observed by reversible protein highlighting. *Science* 306, 1370–1373
31 Shaner, N.C. *et al.* (2004) Improved monomeric red, orange and yellow fluorescent proteins derived from Discosoma sp. red fluorescent protein. *Nat. Biotechnol.* 22, 1567–1572
32 Patterson, G.H. and Lippincott-Schwartz, J. (2004) Selective photolabeling of proteins using photoactivatable GFP. *Methods* 32, 445–450
33 Calvert, P.D. *et al.* (2007) Fluorescence relaxation in 3D from diffraction-limited sources of PA-GFP or sinks of EGFP created by multi-photon photoconversion. *J. Microsc.* 225, 49–71
34 Ivanchenko, S. *et al.* (2007) Two-photon excitation and photoconversion of EosFP in dual-color 4Pi confocal microscopy. *Biophys. J.* 92, 4451–4457
35 Vaziri, A. *et al.* (2008) Multilayer three-dimensional super-resolution imaging of thick biological samples. *Proc. Natl. Acad. Sci. U. S. A.* 105, 20221–20226
36 Kim, P.K. *et al.* (2006) The origin and maintenance of mammalian peroxisomes involves a *de novo* PEX16-dependent pathway from the ER. *J. Cell Biol.* 173, 521–532
37 Hailey, D.W. and Lippincott-Schwartz, J. (2009) Using photoactivatable proteins to monitor autophagosome lifetime. *Methods Enzymol.* 452, 25–45
38 Christensen, N.M. *et al.* (2009) Evidence for unidirectional flow through plasmodesmata. *Plant. Physiol.* 150, 96–104
39 Ferenz, N.P. and Wadsworth, P. (2007) Prophase microtubule arrays undergo flux-like behavior in mammalian cells. *Mol. Biol. Cell* 18, 3993–4002
40 Colakoglu, G. and Brown, A. (2009) Intermediate filaments exchange subunits along their length and elongate by end-to-end annealing. *J. Cell Biol.* 185, 769–777
41 Wacker, S.A. *et al.* (2007) A green-to-red photoconvertible protein as an analyzing tool for early vertebrate development. *Dev. Dyn.* 236, 473–480
42 Leung, K.M. *et al.* (2006) Asymmetrical beta-actin mRNA translation in growth cones mediates attractive turning to netrin-1. *Nat. Neurosci.* 9, 1247–1256
43 Mavrakis, M. *et al.* (2009) Plasma membrane polarity and compartmentalization are established before cellularization in the fly embryo. *Dev. Cell* 16, 93–104
44 Bergeland, T. *et al.* (2008) Cell-cycle-dependent binding kinetics for the early endosomal tethering factor EEA1. *EMBO Rep.* 9, 171–178
45 Deryusheva, S. and Gall, J.G. (2004) Dynamics of coilin in Cajal bodies of the Xenopus germinal vesicle. *Proc. Natl. Acad. Sci. U. S. A.* 101, 4810–4814
46 Schmierer, B. and Hill, C.S. (2005) Kinetic analysis of Smad nucleocytoplasmic shuttling reveals a mechanism for transforming growth factor beta-dependent nuclear accumulation of Smads. *Mol. Cell Biol.* 25, 9845–9858
47 Demarco, I.A. *et al.* (2006) Monitoring dynamic protein interactions with photoquenching FRET. *Nat. Methods* 3, 519–524
48 Hess, S.T. *et al.* (2006) Ultra-high-resolution imaging by fluorescence photoactivation localization microscopy. *Biophys J.* 91, 4258–4272
49 Egner, A. *et al.* (2007) Fluorescence nanoscopy in whole cells by asynchronous localization of photoswitching emitters. *Biophys J.* 93, 3285–3290
50 Rust, M.J. *et al.* (2006) Sub-diffraction-limit imaging by stochastic optical reconstruction microscopy (STORM). *Nat. Methods* 3, 793–795
51 Bates, M. *et al.* (2008) Super-resolution microscopy by nanoscale localization of photoswitchable fluorescent probes. *Curr. Opin. Chem. Biol.* 12, 505–514
52 Lippincott-Schwartz, J. and Manley, S. (2009) Putting super-resolution fluorescence microscopy to work. *Nat. Methods* 6, 21–23
53 Hess, S.T. *et al.* (2007) Dynamic clustered distribution of hemagglutinin resolved at 40 nm in living cell membranes discriminates between raft theories. *Proc. Natl. Acad. Sci. U. S. A.* 104, 17370–17375
54 Greenfield, D. *et al.* (2009) Self-organization of the *Escherichia coli* chemotaxis network imaged with super-resolution light microscopy. *PLoS Biol.* 7, e1000137
55 Gustafsson, M.G. *et al.* (2008) Three-dimensional resolution doubling in wide-field fluorescence microscopy by structured illumination. *Biophys. J.* 94, 4957–4970
56 Huang, B. *et al.* (2008) Three-dimensional super-resolution imaging by stochastic optical reconstruction microscopy. *Science* 319, 810–813
57 Juette, M.F. *et al.* (2008) Three-dimensional sub-100 nm resolution fluorescence microscopy of thick samples. *Nat. Methods* 5, 527–529
58 Schmidt, R. *et al.* (2008) Spherical nanosized focal spot unravels the interior of cells. *Nat. Methods* 5, 539–544
59 Pavani, S.R. *et al.* (2009) Three-dimensional, single-molecule fluorescence imaging beyond the diffraction limit by using a double-helix point spread function. *Proc. Natl. Acad. Sci. U. S. A.* 106, 2995–2999
60 Shtengel, G. *et al.* (2009) Interferometric fluorescent super-resolution microscopy resolves 3D cellular ultrastructure. *Proc. Natl. Acad. Sci. U. S. A.* 106, 3125–3130
61 Shroff, H. *et al.* (2008) Live-cell photoactivated localization microscopy of nanoscale adhesion dynamics. *Nat. Methods* 5, 417–423
62 Biteen, J.S. *et al.* (2008) Super-resolution imaging in live *Caulobacter crescentus* cells using photoswitchable EYFP. *Nat. Methods* 5, 947–949
63 Manley, S. *et al.* (2008) High-density mapping of single-molecule trajectories with photoactivated localization microscopy. *Nat. Methods* 5, 155–157
64 Niu, L. and Yu, J. (2008) Investigating intracellular dynamics of FtsZ cytoskeleton with photoactivation single-molecule tracking. *Biophys. J.* 95, 2009–2016